Pure Appl. Geophys. 173 (2016), 1243–1264

DOI 10.1007/s00024-015-1182-y

Pure and Applied Geophysics

Gravity for Detecting Caves: Airborne and Terrestrial Simulations Based on a Comprehensive Karstic Cave Benchmark

Carla Braitenberg,[1] Daniele Sampietro,[2] Tommaso Pivetta,[1] David Zuliani,[3] Alfio Barbagallo,[3] Paolo Fabris,[3] Lorenzo Rossi,[4] Julius Fabbri,[1] and Ahmed Hamdi Mansi[4]

Abstract—Underground caves bear a natural hazard due to their possible evolution into a sink hole. Mapping of all existing caves could be useful for general civil usages as natural deposits or tourism and sports. Natural caves exist globally and are typical in karst areas. We investigate the resolution power of modern gravity campaigns to systematically detect all void caves of a minimum size in a given area. Both aerogravity and terrestrial acquisitions are considered. Positioning of the gravity station is fastest with GNSS methods the performance of which is investigated. The estimates are based on a benchmark cave of which the geometry is known precisely through a laser-scan survey. The cave is the Grotta Gigante cave in NE Italy in the classic karst. The gravity acquisition is discussed, where heights have been acquired with dual-frequency geodetic GNSS receivers and Total Station. Height acquisitions with non-geodetic low-cost receivers are shown to be useful, although the error on the gravity field is larger. The cave produces a signal of -1.5×10^{-5} m/s^2, with a clear elliptic geometry. We analyze feasibility of airborne gravity acquisitions for the purpose of systematically mapping void caves. It is found that observations from fixed wing aircraft cannot resolve the caves, but observations from slower and low-flying helicopters or drones do. In order to detect the presence of caves the size of the benchmark cave, systematic terrestrial acquisitions require a density of three stations on square 500 by 500 m^2 tiles. The question has a large impact on civil and environmental purposes, since it will allow planning of urban development at a safe distance from subsurface caves. The survey shows that a systematic coverage of the karst would have the benefit to recover the position of all of the greater existing void caves.

Key words: Terrestrial gravity acquisition, airborne gravity, cave detection, Grotta Gigante cave, RTK GNSS positioning.

1. Introduction

The Grotta Gigante cave (NE Italy) is located in the classical karst shared between NE Italy and SW Slovenia (Fig. 1), which is the region which gave the name to analogous geologic formations found in many parts of the world. All karst areas have in common the presence of natural caves, of which many are presently undiscovered and not mapped. Here and in the following we intend void caves, in contrast to a possible sediment filling of caves. The void caves are of major interest to us, as their collapse has a much greater impact on the surface morphology than in the case they were filled up with sediments or gravel. The void caves bear a potential hazard, because the rock becomes fragile and can break due to heavy loading and oscillatory stimulation. In Germany, the hazard has been recognized and planned high-velocity train tracks require the geophysical investigation of the underground to detect possible caves. In Italy, legislation requires a geological certification about the stability of a new building ground of civil interest, but does not require any specific control of presence of caves in karstic areas. The risk of cave collapse is presently neglected, and no numerical investigations exist on the stability of the structure in view of loading by buildings or car traffic.

The Grotta Gigante is a good illustration, as over the cave there are buildings as well as a street over which no restriction on traffic exists, but to our knowledge the problem of mechanical stability should yet be done. It is therefore of general interest

Electronic supplementary material The online version of this article (doi:10.1007/s00024-015-1182-y) contains supplementary material, which is available to authorized users.

[1] Department of Mathematics and Geosciences, University of Trieste, via Weiss 1, 34127 Trieste, Italy. E-mail: berg@units.it
[2] GReD s.r.l., c/o ComoNExT via Cavour 2, 22074 Lomazzo, CO, Italy.
[3] Istituto Nazionale di Oceanografia e di Geofisica Sperimentale, via Treviso 55, 3100 Udine, Italy.
[4] DICA, Politecnico di Milano, Piazza Leonardo da Vinci 32, 20133 Milan, Italy.

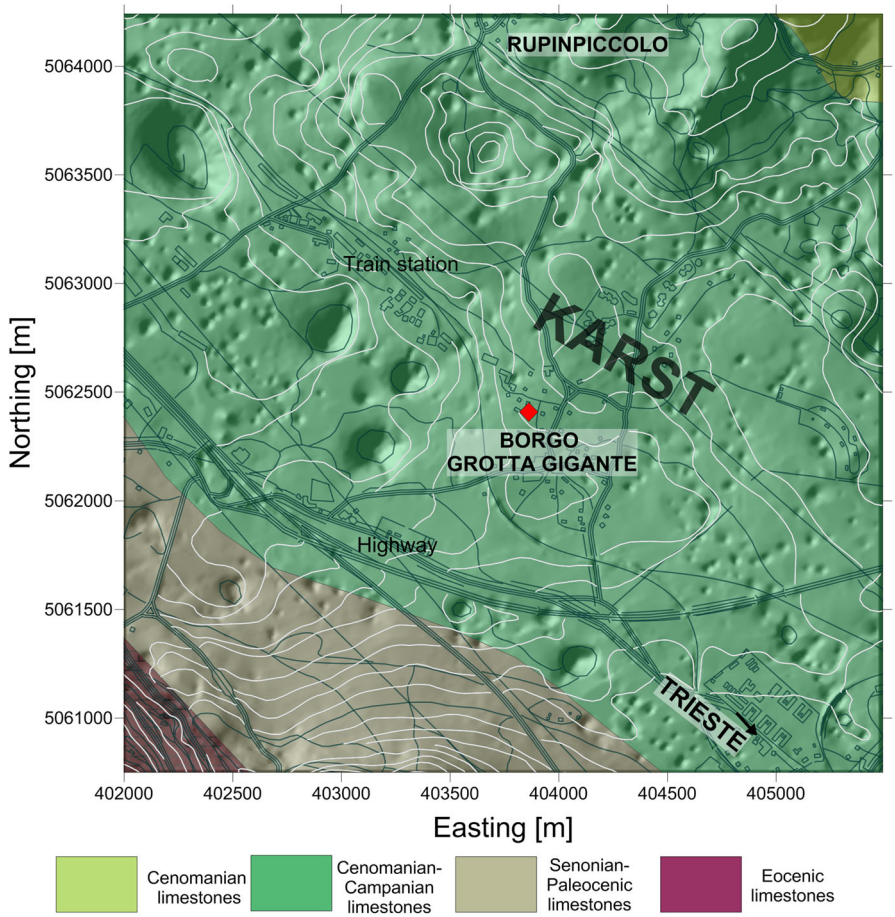

Figure 1

High resolution topography (Regional DEM) over the Italian Karst demonstrating the presence of many sink holes. The location of the map corresponds to the black square in the Fig. 2b. The sink holes have been formed by collapsed caves. Main human infrastructures and urbanized areas from the regional technical cartography are superposed too. A simplified geologic map is reported in transparence, showing high geologic control in this area for the development of karstic forms (data from Regione Autonoma Friuli Venezia Giulia, 2006)

to set up the premises of the data necessary for a numerical modeling, which include geometry, density and mechanical parameters. A further question of interest is whether the cave continues at either end of its extremes, which could be expected due to the erosional action of the hydrologic surface and subsurface runoff. Another question is the planning of a systematic gravity acquisition so as to detect all existing caves of a given size in the region. We use the gravimetric investigation method to map the mass deficit of the cave through the gravity field measured at the surface. The relevance of the dataset we present and publish goes beyond the case history of this particular cave, because it can be used as a benchmark dataset to verify the sensibility of gravity measurements for detecting caves and to test inverse and forward gravity methodologies and software. We owe this broader importance to the precisely known geometry of the cave, which has been recently mapped with a 3D laser-scan investigation. In a companion paper (Pivetta and Braitenberg 2015) we discuss how the laser-scan data are converted to a solid 3D model of the cave, which together with the gravity values discussed here form a unique benchmark dataset. Here we describe the gravity campaign, including the GNSS methods used for positioning the stations in real time kinematic and post-processing acquisition mode. Relative accuracy and difference in

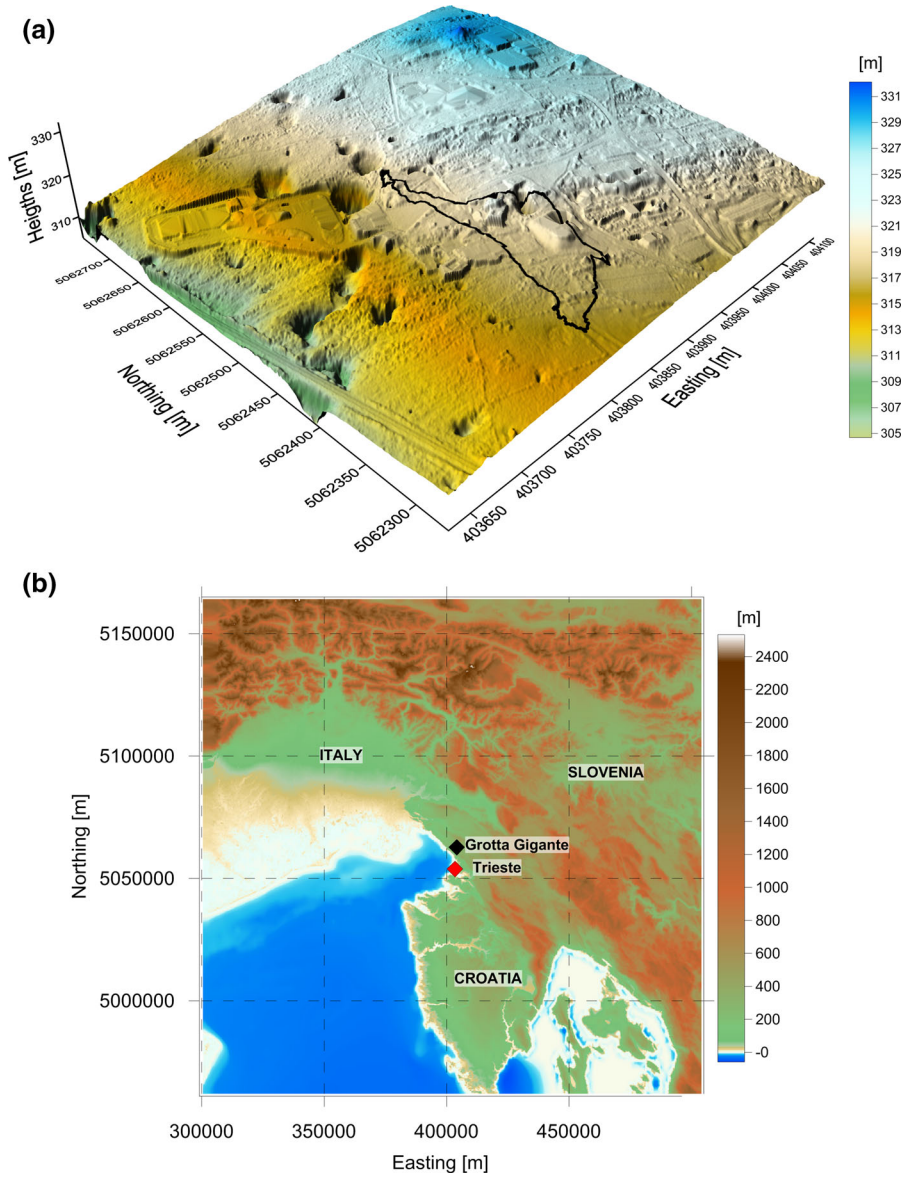

Figure 2

Detailed and regional DEM of the area. **a** Map of DEM of laser-scan survey (PAGANINI and PAVAN 2012) above the cave on an area of about 450 m × 450 m. *Black line* is outline of the cave. **b** Map of the far field digital elevation model (SRTM, Shuttle Radar Topography Mission) used in the topographic reduction of the observations. The outline of the Friuli Venezia-Giulia Municipality and the location of the town of Trieste are also displayed

horizontal and vertical coordinates are discussed, as well as the gravity field observations and reductions. The area bears some challenges in the topographic reduction due to the narrow strip of homogeneous data limited by the Adriatic Sea to the west and by the Slovenian-Italian border to the east. This is a common situation to all coastal areas and areas close to a national border. National borders present a problem as the resolution and precision of the acquired datasets are country-specific; furthermore, datum shifts due to different height systems and different Cartesian systems may exist. We discuss whether an airborne survey could detect similar big caves, with great reduction in the necessary time of

acquisition. We further investigate which station density is necessary to detect caves of a given size with terrestrial observations. Here the benchmark of the cave is necessary, as we have a realistic geometry and gravity signal of the cave.

The database of the volume of the cave and the gravity data can be used in the future for software testing and teaching, as they illustrate in a very intuitive manner what a gravity field responds to. In this case the much-cited ambiguity of the potential field method does not apply, and the gravity field can be well used to obtain information on the concealed cave.

2. The Scientific and Touristic Grotta Gigante Cave

The Classic Karst extends 40 km in length and 15 km in width, with 550 km^2 in Slovenia and 200 km^2 in Italy, and extension of karstification over a thickness of at least 600 m. The term "Classic" Karst distinguishes this area from the many other worldwide karstic areas by the fact that here the first karst studies were made in the beginning of eighteenth century (Ford and Williams 2007). The Classic Karst is part of the Triassic to Eocene Carbonatic platform belonging to the Adriatic plate (Cucchi *et al*. 2001). Based on the Kadastre of the Regione Friuli Venezia Giulia there are 3170 caves in the Italian Karst sector, of which more than 150 extend for more than 100 m and about 10 develop over a length of the order of a kilometer. There are over 80 dolines with diameter greater 100 m and the karrenfields cover an area of several tens of square kilometers. The geometries are very different, and can be of horizontal development, near to vertical shafts, and open spaces over 100 m deep. The density of caves and dolines in the Italian Karst is greatest along an axis parallel to the coastline, and corresponds to the Turonian–Senonian limestones (Aurisina Limestones). The maximum distribution could be tied either to the subsurface water flow or to the reduced resistance to erosion of this formation (Visintin 2011). This line is evident on the high-resolution topography, where an elevated number of circular features is seen, representing sink holes (Fig. 1). The karstification bears a hazard due to possible appearance of sink holes, events in which the top of an eroded volume collapses, leaving a depression in the ground.

The Grotta Gigante cave is used both touristically and scientifically. It is open to the public and fully accessible by foot. The cave is constituted by a wide ellipsoidal hall 100 m long, 60 m wide and almost 100 m high and is connected to the surface through two tunnels. Projecting the outline of the cavity structure onto the surface it results over 250 m long. A near to vertical shaft at the lowest section of the cave is 180 m deep, extending to 10–15 m above sea level. The scientific instrumentation monitors geodetic, seismologic, environmental and biological parameters. The underground position creates a relatively quiet environment ideal for precision measurements. The first edition of long base geodetic horizontal pendulums was installed 1959, after which the definitive instruments have been measuring tilt continuously since 1964, producing a unique time series of 50 years of tilt observations (Braitenberg et al. 2006). Achievements have been the recording of mega-earthquakes starting with the Chile 1960, including the Sumatra–Andaman earthquake of 2004 and the Tohoku earthquake of 2011 (Park *et al*. 2005; Braitenberg and Zadro 2007). The tiltmeters have been proven also useful in studying the karstic subsurface waterflows which generate a tilt signal (Tenze *et al.* 2012) and other causes that generate tilting are illustrated in (Braitenberg and Nagy 2014). Flow is governed by the fissures and cracks in the first few meters of the karst and through large conduits at greater depths (Devoti *et al*. 2015). The flow characteristics are therefore difficult to study by traditional hydrologic techniques and geodetic methods as tilt measurements and gravity become an alternative investigation method. In this study we consider the static gravity field as a tool to investigate the presence of underground caves.

3. The Laser-Scan Data

In 2011, the Istituto Nazionale di Oceanografia e Geofisica Sperimentale (OGS) acquired a laser-scan dataset which aimed to produce a high-resolution mapping of the cave's internal morphologies. The

OGS campaign was planned to fulfill different objectives, as it could be of great interest for scientific scopes, and was the indispensable base for the creation of a virtual tour of the cave, particularly important for tourism promotion and for allowing the visit of the cavity also to people with motoric disabilities (Fingolo *et al*. 2011).

The laser-scan technique has led to an outstanding representation of the main hall and the entrance and exit tunnels of the Grotta Gigante (Paganini and Pavan 2012). Prior to the internal acquisition an airborne laser-scan survey was conducted in order to get a general geographical and morphological setting. An area of about 450 m × 450 m was investigated, and a detailed point-cloud representation (over 15 points/m^2) of the dolines and karrenfields that surround the cave has been produced (Fig. 2).

Then the internal mapping phase began; however, since GPS data could not be exploited inside the cave, an internal topographic reference system of about 70 benchmark points was established with classical geodetic techniques. Subsequently, leaning on this internal reference network, the laser-scan survey was realized: over 4.5 billion points were acquired and led to a representation of the cavity with a resolution of over 10,000 points/m^2 and a sub-centimetric accuracy (Fingolo *et al*. 2011). Video and photo images in high definition were collected as well. Afterwards all the point clouds were merged together and georeferenced; a subsequent elaboration phase permitted a first reduction of the data density and the filtering of some outliers. Then each data point has been colored using high definition photographs to create a realistic imaging for the virtual tour.

In Fig. 3 some topographic sections across the main morphological axes of the cave and a 3D view of the whole point-cloud dataset are presented. The data processing of the laser-scan data, which are affected by multiples, is explained in Pivetta and Braitenberg (2015). Owing to this laser-scan survey the cave has been correctly located in the 3D space for the first time and its volume has been re-estimated. The Grotta Gigante extends from the entrance gallery to the end of the wide ellipsoidal hall for some 250 m, and has a maximum width of almost 60 m. The top of the vault is about 10 m below the surface and is 100 m above the base of the cave. Fingolo *et al*. (2011) found that the cave's volume is about 360,000 m^3.

The laser-scan dataset, with its impressive characteristics in terms of precision and resolution in the reconstruction of cave's morphology, represents an excellent geometric constraint for a forward modeling analysis of the gravity field. In the companion paper to this study (Pivetta and Braitenberg 2015) we present a new 3D density model derived from the laser-scan survey. We have exploited the prism discretization to construct the 3D model that is used to calculate the gravity anomalies at the same points where gravity has been measured.

The transition from the laser-scan point-cloud to the prism model presented some challenges due to the spatial inhomogeneity of laser-scan data and the computational efforts needed to handle and elaborate such a big dataset. In addition to this, the point-could was not divided between roof and ground surfaces, so a proper method was developed to separate such interfaces in order to correctly define each prism.

The three stage elaboration process (Pivetta and Braitenberg 2015) involved three different algorithms that allowed to automatically obtain the prism model.

In synthesis:

- the first step computed the average on cells of 0.5 m × 0.5 m to obtain a reduction of the data density;
- the second algorithm exploited a local ellipsoidal fitting to filter out some outliers, that were present in the original laser acquired dataset;
- the last step resulted in the definition of the ground and floor surfaces and then elaborated these surfaces to set the 6 values necessary to define each prism.

The density constraint was derived from the direct measuring of bulk density on 20 collected rock samples. The hydrostatic weighting principle allowed to compute a unique contrast density for air/limestones, which is assigned to each prism.

For details both on the elaboration process of laser-scan and on the density determinations, the reader is referred to the paper from Pivetta and Braitenberg (2015).

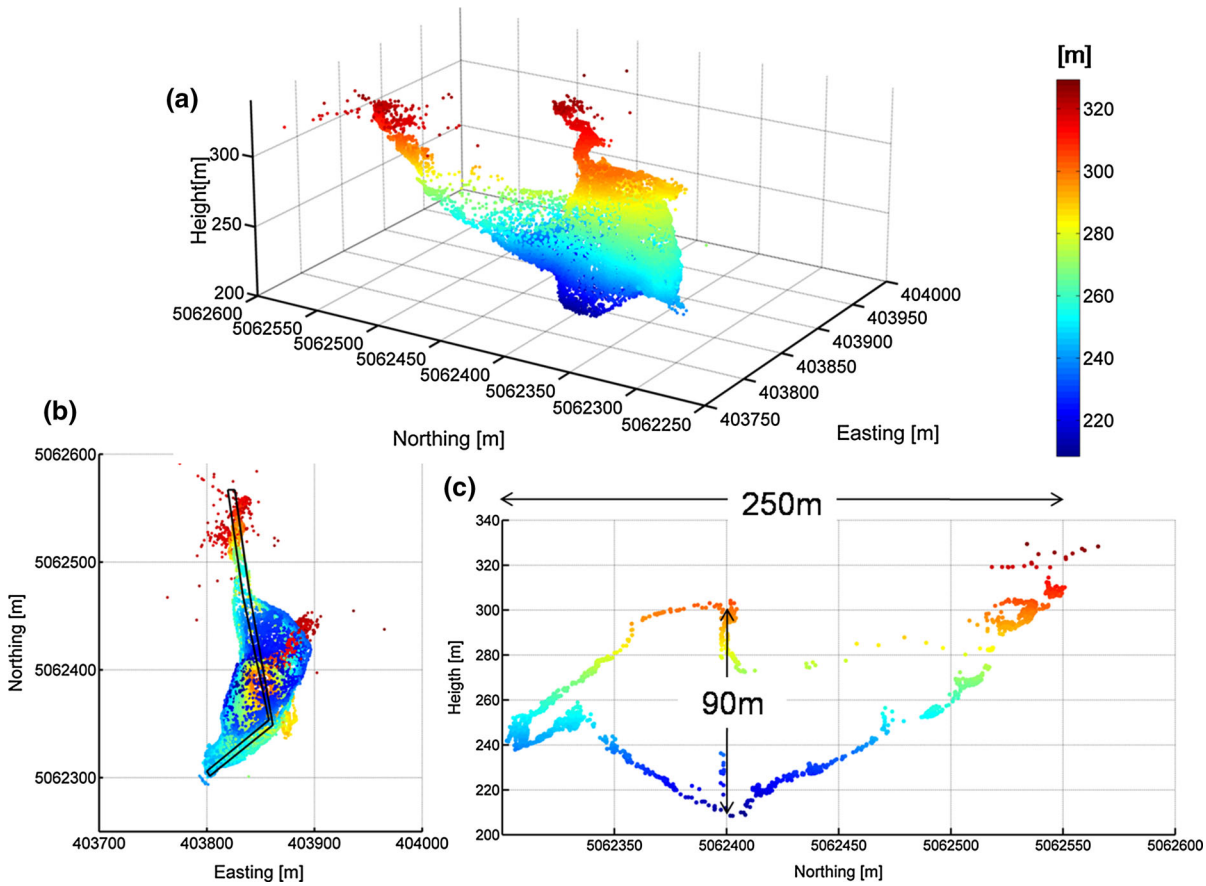

Figure 3
3D illustration of the Grotta Gigante laser-scan acquisition. **a** 3D view from southwest of the Grotta Gigante point-cloud. **b** Plan view of the cave; the *black lines* report the trace of the slice presented in **c**. Note that for a clearer representation the point-cloud density presented has been reduced with respect to the available data

4. *Statistical Evaluation of the Positioning of the Gravity Stations with Different Methods*

The gravity acceleration above the cave has been measured with a relative spring gravimeter (La Coste-Romberg D64), which observes spatio-temporal gravity changes with respect to a fixed reference site. This technique should theoretically allow obtaining precision of the order of the 10^{-8} m/s^2 (10^{-8} m/s^2 is 1 μGal). As a consequence the position of the observation points, and in particular their orthometric height difference with respect to the reference station should be known with a comparable precision. Since, as is well known (Heiskanen and Moritz 1981), the standard free-air gradient, e.g. the rate of change of gravity with height, is of the order of 0.3086×10^{-5} 1/s^2 it turns out that the relative height of each observation point should be known with centimetric accuracy. The actual local knowledge of the geoid as well as new advancement in the positioning technique allow us obtaining this accuracy in different ways.

The position of gravity stations of the Grotta Gigante network has been observed using different techniques and instruments, but always assuring the required accuracy. In this way not only the required point positions have been observed but also different practices have been tested: in particular two geodetic double frequency GNSS receivers (Topcon GRS-1

with PGA-1 + GP geodetic antenna and Leica GX1200) and a Total Station (Leica TS11) have been used.

As for the first GNSS system, i.e. the Topcon receiver, it has been used in Real Time Kinematic (RTK) positioning mode with the antenna mounted on a pole. In this acquisition method a network of permanent GNSS stations broadcasts corrections, mainly for tropospheric and ionospheric delays, over an Internet connection, to the rover receiver (see for instance Hofmann-Wellenhof *et al*. 2008). In detail the Friuli Regional Deformation network, FReDNet (Battaglia *et al*. 2003; Zuliani *et al*. 2003), has been used. This network is mainly used to continuously monitor crustal deformations in the Friuli area and the northeast boundary of the Adriatic microplate. The Friuli area, located within the active collision zone between Eurasia and the Adriatic block, is characterized by one of the strongest clusters of seismic activity in the Adriatic microplate. Relative motions of the Adriatic block and deformation across the Friuli region are up to 4 mm/year. The principal goals of the FReDNet program are to determine the distribution of deformation in this region and to estimate interseismic strain accumulation on its active faults to better assess seismic hazards. The network has several services, e.g. it gives the possibility to download raw GNSS observations in RINEX format and to perform RTK surveys.

The main advantage of the RTK technique is that it allows very fast and accurate surveying: once the signal is received and the ambiguity is fixed with just few observations of the position, we are able to get the coordinates of the point with an accuracy in the order of 2–4 cm. For this experiment we chose to use three position observations for each point. The main problem of an RTK survey is that it requires not only a good sky visibility, as always when using GNSS observations, but also a stable Internet connection.

The second GNSS system, namely the Leica one, has been used in post-processing mode with a fast-static survey. The data are acquired at 1 Hz rate for 15 min in each station and then processed with double differences with respect to two permanent stations: TRIE, belonging to the FReDNet network, and Trieste, part of the Marussi GNSS network maintained by the local government (Regione Friuli Venezia Giulia "A. Marussi"—GNSS network, 2015). The use of the double difference method with respect to a permanent station close to the observed point (i.e. distance smaller than 10 km) the position of which is known with millimeter accuracy is able to remove the error due to GNSS satellite clock's offset and highly reduce tropospheric and ionospheric errors (Leick 2004). Note that the use of two permanent stations not only improves the results in terms of accuracy but also allows to properly estimate the variances of the predicted positions joining the estimated baselines in a least square adjustment.

The last instrument we used is the Total Station (TS), required in the area where vegetation obstructs the sky visibility. In order to estimate positions in the global reference frame the TS observations were combined with GNSS static baselines in a unique least square adjustment by means of the free and open source GeoNet software (Rossi *et al*. 2012; Geonet 2015). This software properly merges TS observations (i.e. distance, azimuth and zenith with respect to the actual plumb line) with GNSS observations in a unique adjustment, directly accounting for the effect of the deflection of the vertical and the Earth curvature.

In summary, the positions of 89 stations have been surveyed with the following scheme (Fig. 4):

- 14 stations with the Topcon RTK GPS system;
- 21 stations with the Leica GNSS receiver (then post-processed);
- 12 stations with the Total Station TS-11;
- 42 stations with Topcon RTK GPS and Leica GNSS systems (then post-processed);
- 10 stations with Leica GNSS receiver (then post-processed) and the Total Station TS-11;
- 5 stations with all the three instruments.

The multiple observations and the different adjustment methods used allow testing the congruence between different positioning methods as shown in Tables 1 and 2.

It can be noticed from the results that the standard deviation in the height direction is always smaller than 2 cm thus assuring 6×10^{-8} m/s^2 level accuracy in the free-air correction. Moreover it can also be observed from the two tables that the largest differences are found in the vertical component between

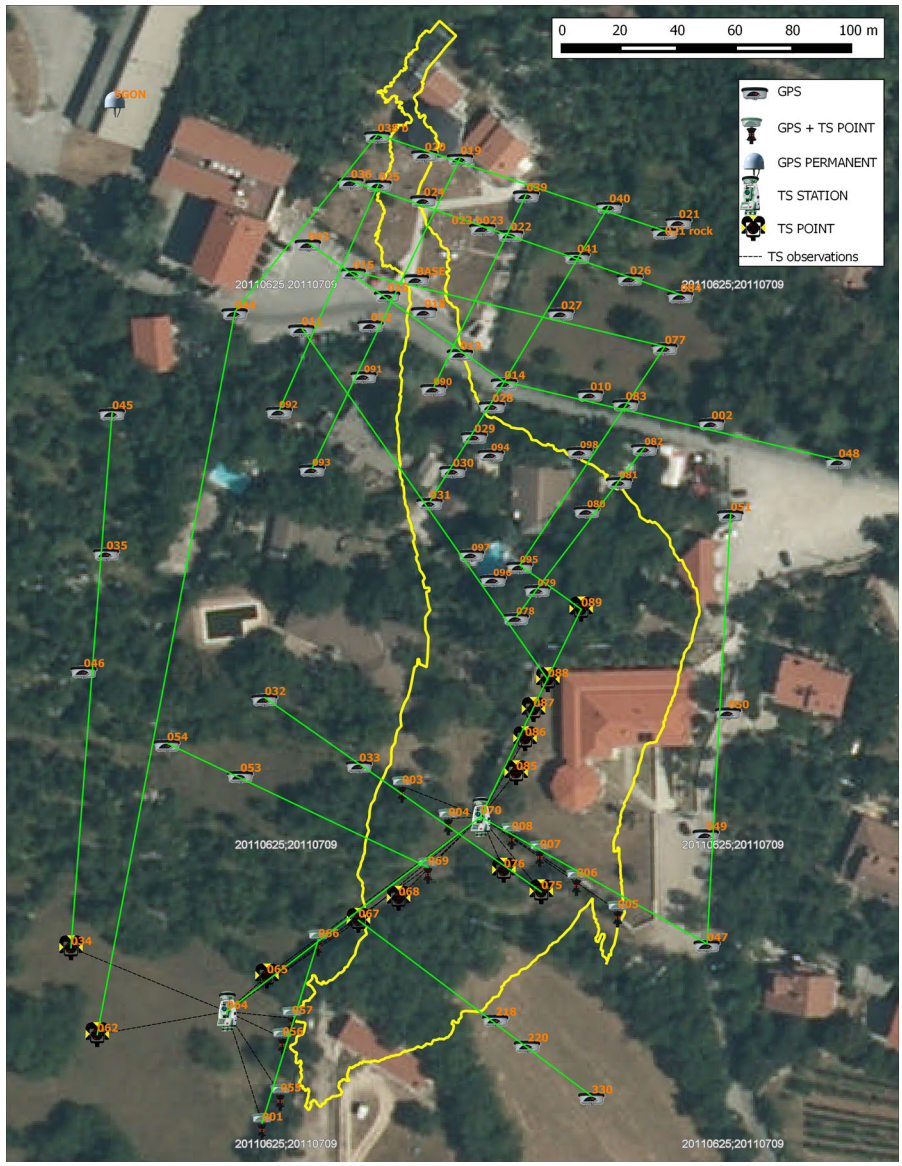

Figure 4
Scheme of observation of height with the different methods: RTK, Leica and Total Station

Table 1

Planar differences between the different positioning methods used in the gravity acquisition

Planar	No. of obs.	Mean (mm)	Std (mm)	Min (mm)	Max (mm)
Leica vs TS	10	−0.4	3	−1.1	1.2
Leica vs Topcon	42	0	17	−10	69

the fast-static and RTK solution. This is due to the fact that a bias, probably due to a different height reference frame or a misalignment of the antennas phase centers, entered in one of the two systems. In any case when dealing with this kind of gravimetric survey we are interested only in the height

Table 2

Height differences between the different positioning methods used in the gravity acquisition

Heights	No. of obs.	Mean (mm)	Std (mm)	Min (mm)	Max (mm)
Leica vs TS	10	−12	16	−17	28
Leica vs Topcon	42	101	13	131	68

differences (since the gravimeter is able to observe only relative variation of the gravity field), and thus a constant bias would not affect the final results. In any case it has been estimated by a least squares adjustment and the RTK positions have been corrected to homogenize the network.

At a time after the gravity acquisition was completed, we investigated whether a non-geodetic receiver (single frequency), namely, a u-blox EVK-6T receiver, could be used for the measurements. This kind of receiver is generally used for low-accuracy navigation and not for precise point positioning, but it has the advantage to be much less expensive (about two orders of magnitude) than the geodetic type. A recent experiment performed by Caldera *et al*. (2015) has shown the possibility to use single-frequency receivers to get millimeter accuracy in the positioning of a static point for geodetic monitoring purposes. Here the dataset from Caldera *et al*. (2015) is analyzed and re-elaborated to prove the possibility of using this low-cost apparatus for gravimetric applications. Basically, the experiment consists in having the u-blox receiver acquiring data for a long period (over a time span of 60 days). The GNSS monitoring equipment was installed in the Media Center, Osaka City University, Japan, which is one of the tallest buildings in the neighborhood, guaranteeing a good sky visibility for receiving GNSS satellite signals. As base stations, a virtual reference station (VRS), generated by the JENOBA positioning service (Wanninger 2003), and a permanent station belonging to GEONET, the nationwide GNSS network of Japan (Tsuji *et al*. 2013) were used. The VRS was generated at a distance of about 60 m from the low-cost antenna. The GEONET station was located at a distance of about 7.5 km thus resembling the Grotta Gigante situation.

Code and phase observations of the low-cost receiver are post-processed by the relative positioning algorithm of goGPS, MATLAB version (Realini and Reguzzoni 2013; Herrera *et al*. 2015), which applies an extended Kalman filter on double-differenced code and phase observations, estimating the antenna coordinates and float carrier phase ambiguities. The LAMBDA3 algorithm (Verhagen and Li 2012; Li *et al*. 2013) was applied epoch-by-epoch on the float ambiguity solutions. The full dataset is processed in order to estimate the position of the u-blox receiver with extremely high (millimetric) accuracy. After that, starting from the whole dataset, we generate and process 15 trial datasets each one containing only 15 min observations. Considering the 60 days solution as the "true" position of the monitored point we estimate the accuracy of all of the 15 min trials.

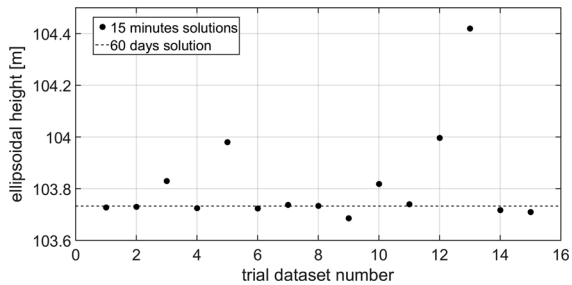

Figure 5
Accuracy of the solutions with the GEONET stations using low-cost one-frequency GNSS receivers

The accuracy of the solutions with the GEONET station is reported in Fig. 5 where it can be seen how the mean difference between the true position and the estimated one is of only 9 cm with a standard deviation of the order of 19 cm. Considering the vertical gravity gradient of 0.3086×10^{-5} 1/s^2, this translates to errors in the final gravitational field smaller than a tenth of 10^{-5} m/s^2. It should be also observed that only one of the 15 datasets used has an error larger than 60 cm. The large error is probably due to a non-perfect processing of cycle slips in the goGPS software. If this outlier is removed from the analysis, the error standard deviation drops to only 8 cm with

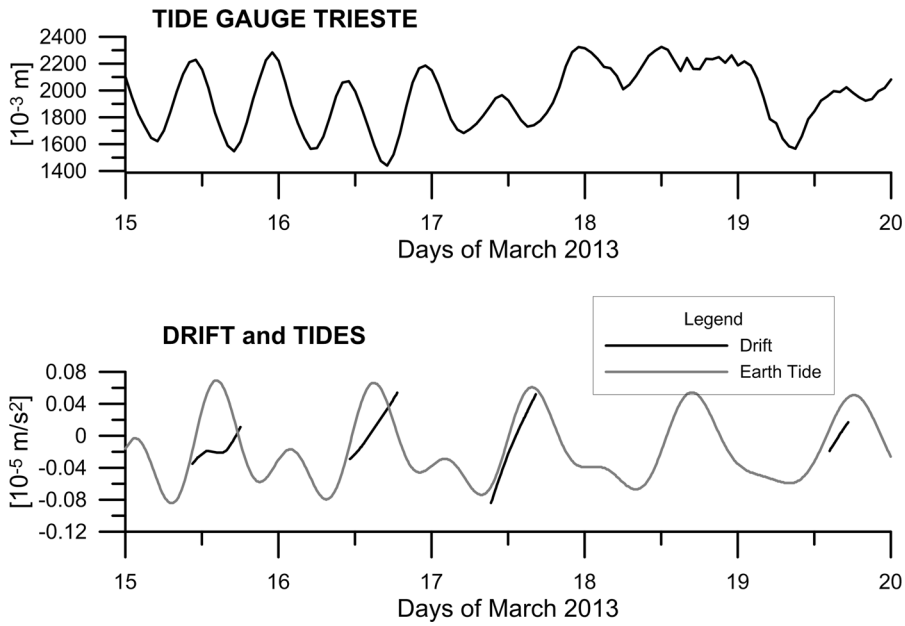

Figure 6
Illustration of instrumental drift reduction of the Grotta Gigante gravity campaign. Theoretical gravity tide (*grey*) and drift curves (*black*). The drift is of the same order of the tides and is always towards an increase in gravity. It is uncorrelated to the sea level of the Adriatic in the Trieste harbor (data courtesy of Dr. Raicich and Dr. Cirilli)

an average error of 3.0 cm. The VRS solution presents similar behavior with a standard deviation of 7.4 cm and an average error of 2.8 cm. This simple experiment demonstrates the possibility of using low-cost single-frequency receiver, properly processed with ad-hoc solutions, to observe coordinates for gravity networks. At the time of the gravity survey the low-cost receivers had not been set into action, so we could not make a direct comparison between the acquired heights from RTK, fast static double frequency and the fast static single frequency solutions. However the above experiment is here reported, because it shows that the new low-cost receivers could be used for analogous gravity investigations.

5. Gravity Field Campaign

The gravity field was measured with a traditional La Coste-Romberg model D relative gravimeter with optical reading (D64). Feedback systems have been mounted to these older systems, but the optical reading has the advantage of greater stability are not in danger an additional drift due to the feedback system.

The measurements were made with the scope of covering the cave in detail and achieving a homogeneous distribution of data-points. From the height stations, in total 75 stations were measured with gravity, distributed over the cave (Fig. 4). As it is seen in this figure, the urbanization and network of streets is independent from the outline of the cave, so due to the numerous private constructions and properties, access was not possible everywhere.

5.1. Tidal Corrections, Drift Curves

The raw gravity observations are corrected for the earth tides and drift with the dbGrav software written and distributed by Dr. Sabine Schmidt (personal communication, 2015), University of Kiel, Germany. In Fig. 6 the earth tide and drift are graphed for the four days spanning the data acquisition (15–19 March 2013). The drift is modeled as a spline curve by the software, and the operator chooses a weight parameter which affects the stiffness of the curve. The drift is defined by the repeat measurements during data acquisition, which have been made on a 30 % basis, meaning that 30 % of all measurements were made

on a station that had been occupied before. We choose systematically a stiff curve, allowing only moderate deviation from linearity. There is no physical criterion to define the stiffness of the drift, as the drift may be affected by inadvertently moving the instrument. The drift is systematically in one direction, increasing the gravity value, with an average rate $0.012 \pm 0.006 \times 10^{-5}$ m/s^2/h. The loading and gravitational effect of the Adriatic has not been corrected, because to our knowledge a reliable testing of available ocean models has not been accomplished up to now for the karst area. Before using existing global ocean loading tide models, it must be checked whether the relatively small Adriatic basin is correctly modeled. The tides in the Trieste basin are relatively large, with peak-to-peak amplitudes of over 1 m. They therefore necessitate a dedicated study that examines the gravitational mass and the loading effect, based on the findings of Zadro and Chiaruttini (1975) and on up-to-date hydrologic models of cotidal lines in the Adriatic, leading to the gravity reduction on karst-stations. If not corrected, as is our case, the combined gravimetric and loading effect could contribute to the drift, as emerges from the theoretical calculation for the two major diurnal (K1) and semidiurnal (M2) ocean tides of the Mediterranean (Zadro and Chiaruttini 1975). Adopting the coefficients published in Zadro and Chiaruttini (1975), in the Karst the effect amounts to about 0.006×10^{-5} m/s^2 for each of the two major tides, so the maximum effect given when the two waves are in-phase is 0.012×10^{-5} m/s^2. Considering a time of 12 h, the drift amounts to maximum 0.002×10^{-5} m/s^2/h. This value is just a bit lower than the order of magnitude of the drift we observe, so an influence cannot be excluded. It cannot be the prevailing signal, since the drift is always in one direction, whereas the tidal signal should change sign. Furthermore the drift and the observed sea level obtained from a tide gauge in the Trieste harbor do not correlate (Fig. 6).

We have made a control measurement in the lab leaving the instrument fixed in the same position for 4 days. Again we find a drift in the same direction, increasing the gravity value with time and drift rate of 0.005×10^{-5} m/s^2/h (Fig. 7). The figure shows the tide gauge in Trieste harbor (top), the linear fit to the observations (middle) and the short term spline interpolated drift curves (bottom) together with gravity earth tides and residual from drift curve. The linear fit was made with 49 samples and has a coefficient of determination (R^2) of 0.99. The coefficient of determination is defined as:

$$R^2 = 1 - \frac{S1}{S1 + S2} \tag{1}$$

With $S1$ the sum of the squared residuals from the linear interpolation, and $S2$ the variance of the data.

The comparison to the tide gauges in the harbor of Trieste again does not reveal a correlation between the sea level and the drift of the gravimeter.

5.2. *Complete Bouguer Topographic Reduction*

The 75 free-air gravity values should be corrected for the gravitational effect of topography and bathymetry in order to obtain the Bouguer field. Here and in the following we do not separate the simple (infinite flat Bouguer plate) and complete Bouguer (terrain correction) reduction in two steps. The digital terrain model allows the calculation of the gravitational effect of topography and the water placed between the reference surface and the ocean bottom at any point in 3D space, and considering any maximum radius of interest. There is no advantage in dividing the calculation in two steps, the Bouguer infinite plate reduction and the classic topographic reduction, necessary to correct for the erroneous infinite plate. We rather consider the complete effect of bathymetry and topography, defining it the topographic reduction. We build a prism model from the available digital elevation models (DEM) and calculate its gravity effect in the same points where gravity data have been observed, obtaining the complete topographic effect. The normal gravity values, the tidal correction and the complete topographic effect are then subtracted.

As already hinted, the area of study lies between the Adriatic Sea and the Italian-Slovenian Border, which are both limits to the homogeneity and usage of DEMs: for instance some topographic models do not include sea bathymetry data, and the coverage area for high resolution models is limited by the political borders. To overcome these problems we

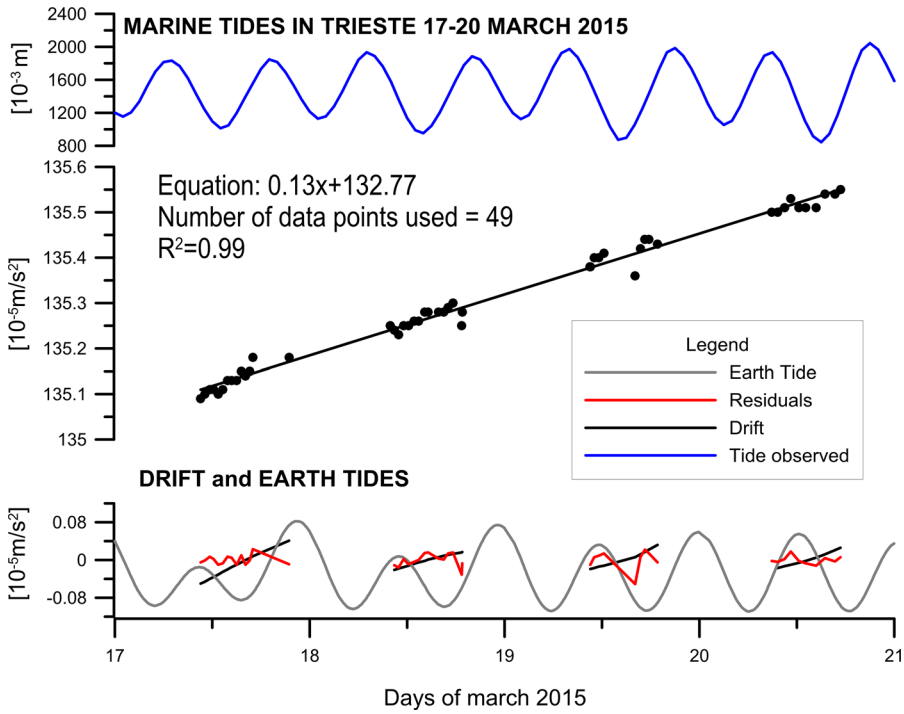

Figure 7
Gravity observations conducted in the Trieste laboratory from 17 to 20 March 2015. *Top* Adriatic sea level measured at the Trieste harbor (data courtesy of Dr. Raicich). *Centre* interpolated drift curve for the 4 days. *Bottom* earth tide gravimetric effect (*grey curve*), daily drift (*black line*), gravity measurement residuals corrected for earth tide and drift effects (*red line*)

have to juxtapose four different topographic datasets with different spatial resolutions. For the area immediately above the cave (450 m × 450 m) we rely on the ALS (airborne laser-scanning) survey that accurately mapped the superficial karstic morphologies. The survey was acquired by the OGS contextually to the internal laser-scan measurements, and allowed to reproduce the topography with 15 million points and an average datum density of 6 points/m^2 (Paganini and Pavan 2012). The data are provided in ASCII digital files in UTM33/WGS84 coordinates of ellipsoidal heights. According to our scopes, the point cloud has been re-sampled to a regular grid of 1 m × 1 m of resolution by averaging. There was no need to treat outliers or multiples as was the case for the data inside the cave.

The second dataset is the regional digital elevation model and has been used to reconstruct the topography of the Italian part of the Karst Plateau, excluding the bathymetry of the Trieste Gulf. The model covers an area of about 9 km^2 around the ALS survey and has a resolution of 10 m. Also this topographic data are given in ASCII digital files where the plane coordinates of the points are expressed in UTM33/WGS84 but the quotas are in orthometric heights.

Finally the more exterior areas have been included merging an offshore bathymetry model, produced by the European Marine Observation and Data Network (EMODnet.eu), and inland topography of the Shuttle Radar Topography Mission (SRTM). The first model reconstructs the bathymetry of the Adriatic Sea with a 250 m resolution, the second the worldwide topographic model of onshore areas with maximum resolution of 90 m acquired from the Space Shuttle (Farr *et al*. 2007). Data are provided in geodetic WGS84 coordinates and orthometric heights. To obtain a uniform grid, the SRTM has been resampled to EMODnet resolution, and its areal coverage has been extended about 1° around the Trieste municipality.

All the datasets have been homogenized to the same reference system. The plane coordinates of the

various digital models have been transformed to UTM33/WGS84 system and the orthometric heights have been corrected for the geoidal undulation (from EGM96 model) obtaining the ellipsoidal heights. Although the GOCE-derived geoid has superior precision and resolution compared to EGM96, we must add the same geoid which was used originally for converting measured ellipsoidal heights to orthometric heights. The topographic reduction is made with a 1 m near field grid, a 10 m moderately near grid, and a 250 m regional grid for the far field. The different topographic datasets are published online as supplementary material to the paper.

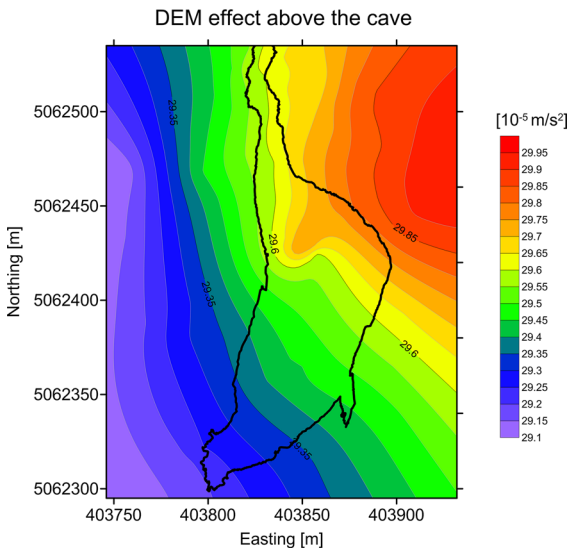

Figure 8
Topographic reduction for the stations above the Grotta Gigante cave. The effect considers the DEM up to a distance of 1°

The prism model is then easily constructed and its gravity effect, which has been calculated in the same points where gravity was observed, is shown in Fig. 8. The gravity anomaly and the Bouguer anomaly are shown in Fig. 9. The extreme values and standard deviations are given in Table 3.

6. Airborne Gravity for Karstic Cave Detections

The gravity and geometry benchmark dataset of the cave allows us to fulfill a realistic investigation on the possibility of detecting large karstic caves by airborne surveys. The Italian and Slovenian Karst has a number of explored caves, but also a number of completely unknown ones can be expected. An example is the Grotta Impossibile cave, located 10 km southeast of the Grotta Gigante cave and discovered by chance in 2004 during excavations of a

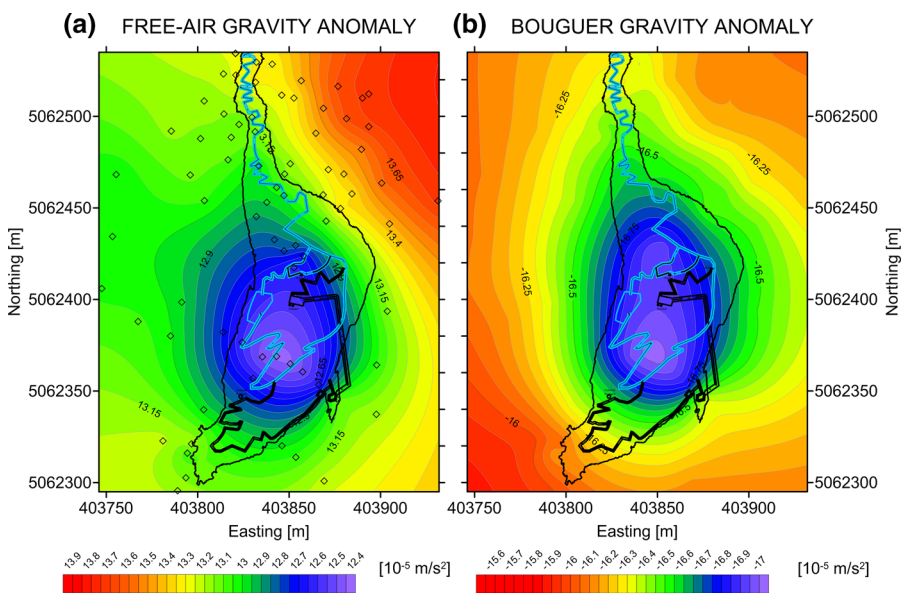

Figure 9
Gravity field of the cave; **a** Free air gravity field **b** Bouguer gravity field. *Black line* outline of cave. *Black lines* inside cave: pathways inside the cave used by tourists. *Black symbols* gravity stations

Table 3

Statistics on height, free air anomaly, Bouguer anomaly, topographic correction for survey points of the gravity measurement campaign

	Min	Max	Average	Standard deviation
Topographic height (m)	315.028	323.408	318.768	1.899
Gravity anomaly (10^{-5} m/s^2)	12.455	13.748	13.135	0.294
Topographic effect (10^{-5} m/s^2)	29.11	29.94	29.55	0.21
Bouguer anomaly (10^{-5} m/s^2)	−17.00	−15.96	16.41	0.26

motor highway tunnel. The Grotta Impossibile cave, which is more than 400 m long with chambers larger than 10,000 m^2 and higher than 80 m, would have been easily detected with a survey similar to the one presented in the current work. In this framework an interesting question is whether it is possible or not to detect similar karstic caves also by means of airborne gravimetry. Airborne gravimetry speeds up the gravitational signal acquisition thus allowing for an economic survey of the whole karst. In order to acquire the 75 ground gravity observations over the area of about 200 × 200 m^2, described in the present work, a couple of days of work has been used. An airborne survey would allow covering areas from 30 km^2 up to 500 km^2 in a single day of campaign. Of course this speed up, combined with a higher altitude, is reflected in a worsening in terms of accuracy and spatial resolution of the observed gravitational field.

In order to assess the possibility to detect caves from airborne gravimetry, a numerical test has been performed. The test consists in the following steps: first of all a set of 14 airborne tracks, seven in the east–west direction and seven in the north–south direction, covering the area of interest, just above the Grotta Gigante cave, with a line spacing of 1 km has been generated. An airplane is simulated to move at a constant velocity of 50 m/s and to acquire gravity data at a rate of 10 Hz, thus giving an observation every 5 m. The aircraft height at each track is computed by interpolating the available DEM and adding a constant of 150 m (150 m above the topography is internationally considered the minimum allowed altitude in uninhabited areas). The flight tracks together with the digital elevation model and the position of the Grotta Gigante cave are shown in Fig. 10.

In order to understand if the cave signal would be detectable at flight altitude it is necessary to simulate

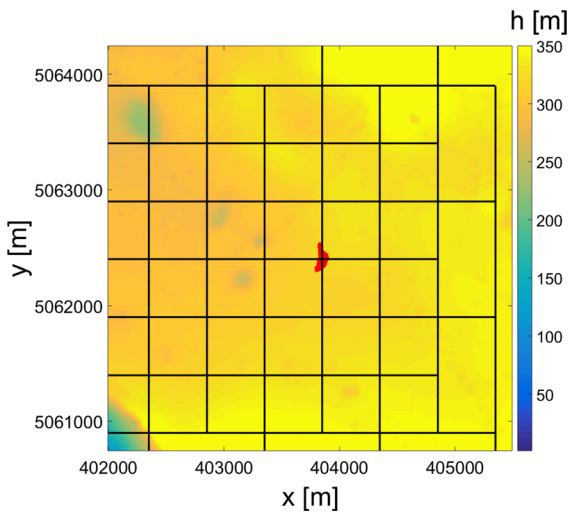

Figure 10
Outline of the simulations for an airborne gravity acquisition. *Thick lines* flight lines. *Red spot outline* of the Grotta Gigante cave. Map of the terrain according to the real digital terrain model

the airborne gravimetry observation noise along the airplane tracks. For this purpose we start from analyzing a real airborne campaign (Department Of Primary Industries, Victoria. 2012) conducted in 2011 as part of the CarbonNet Project by Sander Geophysics Ltd. (SGL) on behalf of the State of Victoria from 23 November to 11 December 2011. The aim of the survey was to provide a better understanding of the onshore, nearshore and immediate offshore geology of the Gippsland Basin (Australia). The survey was performed using SGL AIRGrav system in a fixed wing aircraft (Cessna Grand Caravan 208B). 10,523 line km of data were acquired along flight lines oriented northeast and southwest at 1000 m line spacing and a nine km wide strip along the coast was flown at 500 m line spacing. Tie lines were flown to the northwest and southeast at 10,000 m line spacing. The survey was flown at an

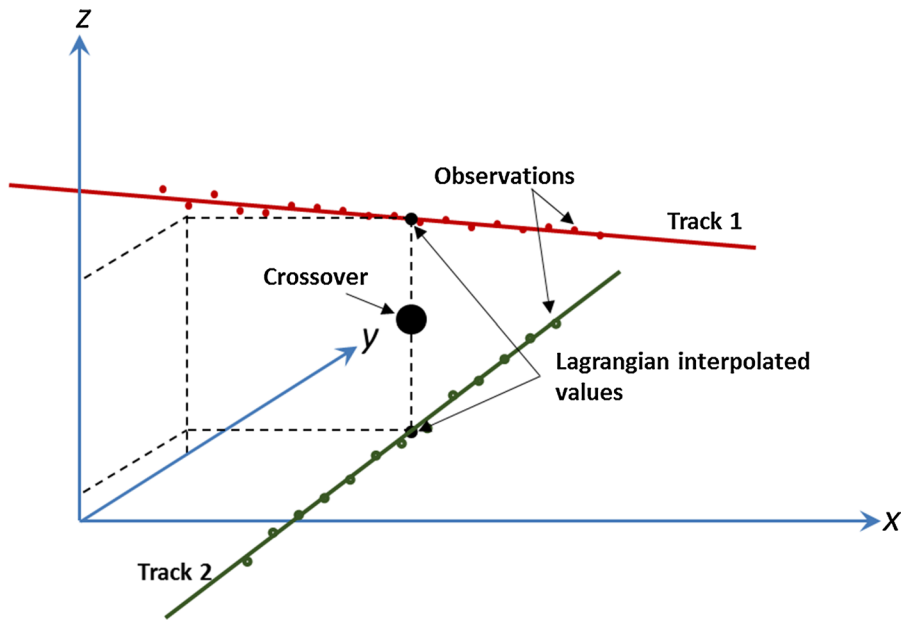

Figure 11
Illustration of the interpolation of the gravity values along two intersecting tracks. As the tracks can have different heights, the values are brought to the same height by calculating the vertical local gravity gradient

average ground speed of 53 m/s, the gravimeter raw observations, recorded at 128 Hz, are first filtered and down sampled to match the 10 Hz GPS measurements. The SGL team therefore computes gravity by subtracting the GPS-derived aircraft accelerations from the inertial ones and applying the Eötvös correction (Harlan 1968).

Starting from the crossovers of this dataset, i.e. the intersection between two perpendicular tracks, a set of 1001 pointwise evaluations of the observation error v has been estimated by computing the difference between the signals at the track intersections. Note that these errors are due not only to the gravimeter observation error, but also to imperfection in the whole procedure applied to estimate the final gravity field, such as mis-modeling in the Eötvös effect or in the computation of the aircraft position.

In any case, to estimate these errors, each track is modeled with a straight line, by means of least squares adjustments, and for each couple of lines the coordinates of the intersection are computed. At this point we interpolate the observations of each line at the crossovers (Fig. 11): first we apply a Lagrangian interpolation (Davis 1975) to predict the gravity value on the modeled line in correspondence of the intersection and, after that, we move the estimated points in the vertical direction by linearizing the problem and computing the second radial derivative of the gravitational potential from the EIGEN-6C4 model (Shako *et al*. 2014). It should be observed that the effect of both these "movements" is quite limited. In fact, the maximum along track shift is smaller than 4 m while in the vertical direction the maximum distance between two tracks at the crossover is of only 1.5 m.

Supposing a homogeneous and isotropic observation error, an empirical covariance function $C_{vv}(d)$, being d the planar distance between two points, was obtained starting from the 1001 samples (Fig. 12). Here the use of the simple planar distance is justified by the relative small variation of the aircraft altitude during the acquisition.

The theoretical covariance $\hat{C}_{vv}(d)$ has been modeled as a series of Bessel functions of the first order (Watson 1995), where the coefficients have been estimated by means of a non-negative least square adjustment (Lawson and Hanson 1974). This would allow obtaining, in an easy and automatic way, an oscillating theoretical covariance function positive definite (Fig. 12).

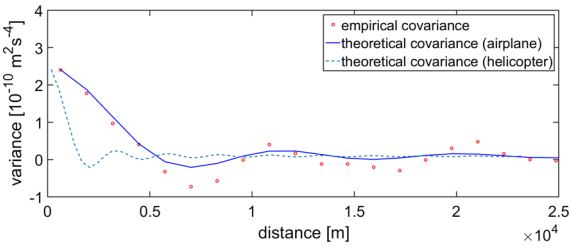

Figure 12
Empirical covariance function $C_{vv}(d)$, being d the planar distance between two points. *Red dots* empirical covariance values. *Blue continuous line* Interpolated covariance function for fixed wing aircraft. *Blue stippled line* estimated covariance function for a helicopter acquisition

As it can be seen the variance of the error is around 3 $(10^{-5}$ m/s$^2)^2$ with a correlation length smaller than 3 km. Note that the presence of such kind of colored noise complicates the separation between signal and noise, and as a consequence the noise removal, for airborne gravity surveys. Once the theoretical covariance of the observation error has been modeled it is possible to generate a realization of the noise on the simulated tracks; this can be simply done by computing the covariance matrix C_{vv} in correspondence of the simulated points. The noise $\hat{v}$ can be simulated as (Franklin 1965; Demeure and Scharf 1987):

$$\hat{v} = Lu \tag{2}$$

where L is the lower triangular matrix from Cholesky decomposition of C_{vv} and u is a vector containing one random extraction from a normal distribution for each observation points.

Note that the deterministic components of the simulated observations, such as the Eötvös effect (which modulus ranges between 39 x 10^{-5} and 540 $\times$ 10^{-5} m/s^2 for the simulated flight), are not computed since we suppose that they can be modeled apart from minor errors. These small errors, as already said above, are however already simulated in the stochastic component computed by means of Eq. 2. The results (shown in Fig. 13) are compared with the gravitational signal of the Grotta Gigante cave computed along the flight tracks by means of the Tesseroids software (Uieda *et al*. 2010, 2011).

From the simulation it can be seen that the Grotta Gigante cave signal is completely masked by the observation noise which results more than one order of magnitude larger.

The whole test has been repeated by simulating observations from a helicopter instead of the airplane. Basically the helicopter allows to reduce the speed from 50 to 18 m/s and the line spacing from 500 to 30 m. We also reduce the flight altitude from 150 m above the topography to only 50 m. In order to compute the empirical covariance of the observation noise, in absence of real helicopter survey data, we use the available airplane campaign. The new empirical covariance can be easily obtained from the old one by rescaling with a factor 2.7 the distance in the abscissa. As it can be seen from Fig. 12, this is reflected in a reduction of the correlation length that

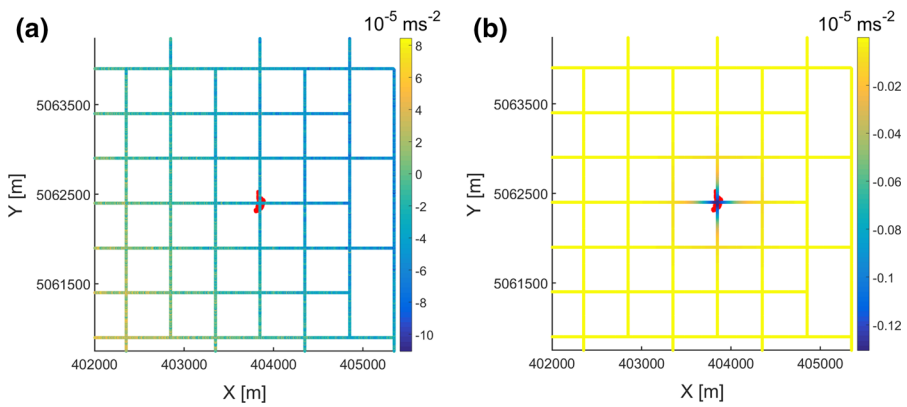

Figure 13
Expected noise level (**a**) for a fixed wing airborne survey and gravity field due to the cave (**b**). The fixed wing survey has a too high noise level and the gravity signal of the cave is masked

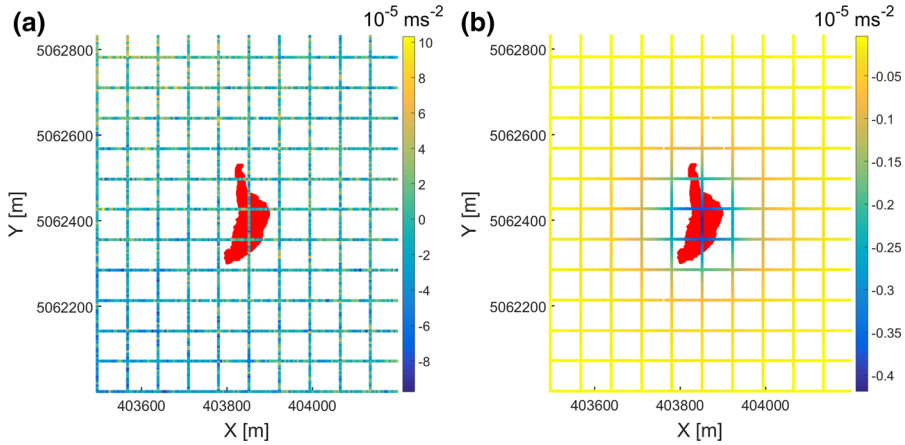

Figure 14

Expected noise level (**a**) for a helicopter airborne survey and gravity field due to the cave (**b**). The helicopter survey has lower noise level and the gravity signal of the cave is near the noise level, but is detectable after some processing

drops for the simulated helicopter survey down to about 1 km. Results from this simulation are shown in the following Fig. 14.

Again the signal is partly masked out by the noise, however the increased resolution of the grid, and the higher cave signal amplitude (due to the lower flight altitude), would facilitate the cave detection. Starting from the simulated observations we estimate by means of a least square solution the best fitting plane and remove it from the data. This basically removes the low frequency noise present in the simulated observations. In order to reduce also the high frequency part of the noise we apply a 50 m moving average to the residual thus obtaining a filtered signal. Finally, to improve the visualization, results have been interpolated on a regular grid by means of a bi-cubic interpolation algorithm (Fig. 15). Here the signal due to the cave can be recognized, however it should be reminded that, this result has been achieved by supposing a very slow and low flight. Moreover simulated data contain only the cave and the observation error and we perfectly know the position of the cave. In a real situation the observation coloured noise as well as possible mis-modeling, such as wrong densities and imperfect digital elevation model can easily hide this small signal. As a consequence the result of this simple test is that probably in order to detect such kind of karstic caves the only applicable solution should be to set up ground gravity campaigns in support of the airborne campaign, which maximize observation accuracy and resolution.

7. *Planning of a Terrestrial Data Acquisition Campaign for the Detection of New Caves*

To conclude our analysis we finally evaluate the detectability of a superficial cave, similar to the Grotta Gigante in terms of size, through an adequate systematic set of ground gravity observations. Assuming a regular grid of acquisition on the corner points of a square of sides L plus the center point of the square, we analyze the probability to detect a cave of spherical volume of radius R or greater (Fig. 16). The figure illustrates how the positioning of the cave relative to the grid points influences the chance to detect a relatively small cave. The number of gravity stations for unit areas is $3/L^2$. The gravity effect of a spherical mass of mass M, set at depth d, at the distance x from the projection of the center point is:

$$g_z = \frac{GMd}{\sqrt{x^2 + d^2}^3} \tag{3}$$

Which we resolve for the square of the distance x:

$$x^2 = \left(\frac{GMd}{g_z}\right)^{2/3} - d^2 \tag{4}$$

We set the gravity g_z equal to the noise level of the Karst area in absence of caves and obtain the

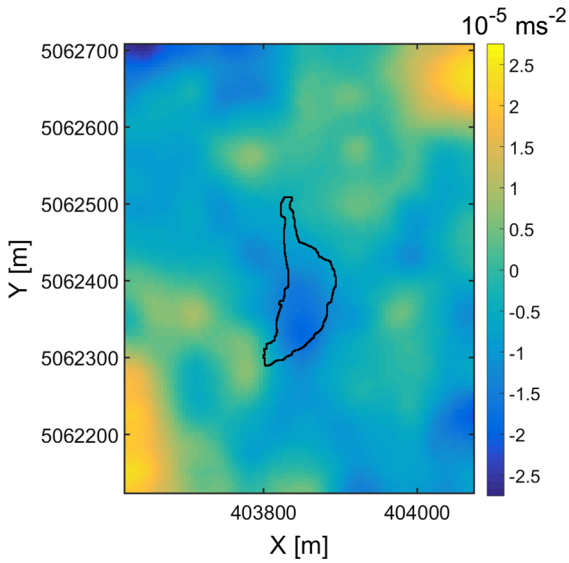

Figure 15
Final processed helicopter survey revealing the presence of the cave. The data are those from the simulation

isoline that corresponds to this noise level. For smaller distances to the projection points the gravity field generated by the cave is stronger than this value. We now calculate the area A_1 subtended by this isoline:

$$A_1 = \pi x^2 = \pi\left(\frac{GMd}{g_z}\right)^{\frac{2}{3}} - \pi d^2 \tag{5}$$

For a spherical cave the mass is related to the radius by:

$$M = \pi\frac{4}{3}\rho R^3 \tag{6}$$

If further the depth is related to the radius and a constant thickness of the cave overburden d_0 we obtain:

$$d = R + d_0 \tag{7}$$

In Fig. 16 the grid of measuring stations is shown, where the stations are set on the four vertices of a square of sides L and in the center of the square. On average there are 3 stations in the area A occupied by the square. The two grey circles show the circular area for which the signal of the cave is greater than the noise level. Two cases are shown, a favorable case (F), with the cave close to one station, and the

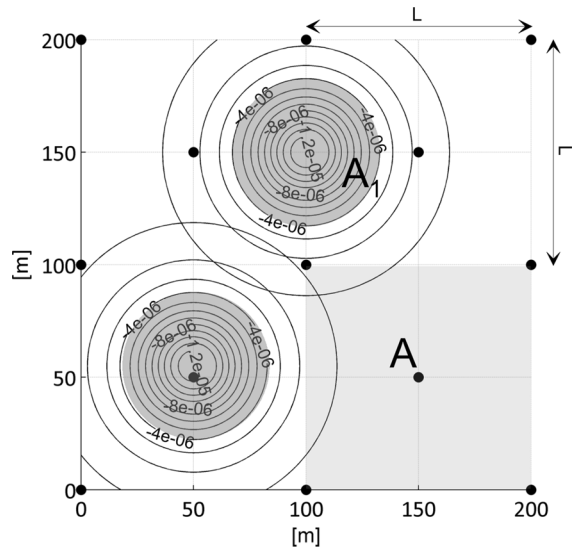

Figure 16
Illustration of a gravity measuring campaign strategy aiming at detecting caves. The station points are placed at the vertices and center of a square area (A) with sides L. *Black dots* gravity stations. The gravity isolines of two caves are shown, one in a favorable (F) and unfavorable (U) position to be detected. *Light grey area* ($A1$) is the area subtended by the isoline corresponding to the noise level. The cave is spherical and has a radius of 25 m, with the *top* at 5 m depth from the surface. Density of the encasing calcareous rocks 2680 kg/m^3

unfavorable (U) case, where the cave is off-centered with respect to the stations.

The probability to detect a cave of radius R is calculated from the probability of having at least 3 stations in the circular area A1 for which the signal is above noise level. Since the number of stations is 3/A, the probability is:

$$p = 3\frac{A_1}{A} \tag{8}$$

If the probability is greater 1, it means that we are sure to detect a cave of a given geometry and depth.

For the case of the Italian Karst we use the above equations to find the probability of detecting a cave of a given radius, and assuming the experimental noise level g_z. We calculate g_z from the gravity values surrounding the Grotta Gigante cave, using an older gravity survey that was more extended than ours but had a lower resolution over the cave (Zanolla *et al.* 1996). We calculate the gravity residual by subtracting the gravity effect of the modeled cave from

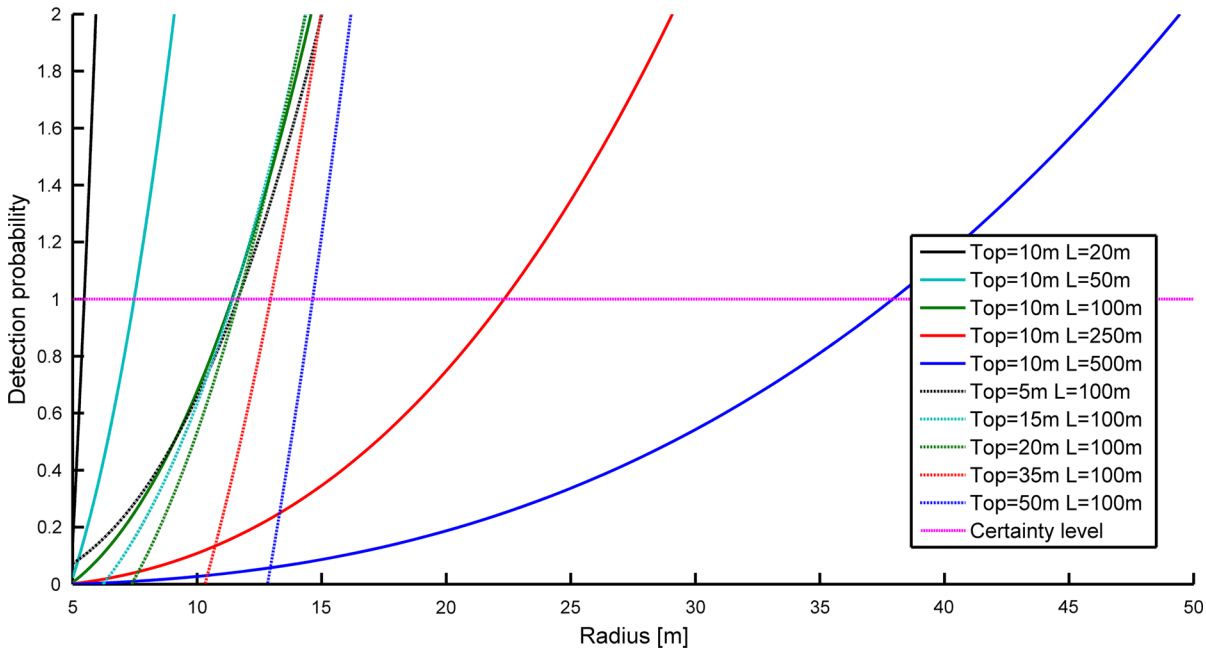

Figure 17
Probability of the detection of a spherical cavity as a function of its radius. Different depths of the sphere's *top* (*dotted lines*) and different resolutions of data acquisition (L; *solid lines*) have been tested. The threshold for the certain detectability level is also reported ($P = 1$)

the observations and then the standard deviation of the gravity residual, which amounts to 0.04×10^{-5} m/s^2. We define the overall noise level to be equal to the standard deviation of the residual. We calculate the probabilities exploring the parameter space, allowing the grid spacing L to vary from 20 to 500 m, and the depth of the top of the spherical cave to vary from 5 to 50 m. The density contrast is set equal to 2680 kg/m^3, the density of the Karst limestones (Pivetta and Braitenberg 2015). The probabilities are plotted against the radius R of the cave. The result is shown in Fig. 17. Two sets of curves are shown, the curves with continuous line leave all parameters constant, but vary the station density (parameter L). The curves with stippled line show the variation of the top of the cave. To be sure to detect the caves of a given radius, the curve must intersect the horizontal line $p = 1$. It is seen that for a grid spacing of 500 m only the biggest caves can be detected, and that with 250 m grid spacing all caves with a radius of 25 m could be detected.

The entire Slovenian and Italian Karst covers an area of 750 km^2, which for a grid spacing of 250 m and 3 points each square results in 36,000 stations. Allowing 15 min measuring time at each station, 30 % double occupancy of the stations, and assuming to have 5 operators equipped each with 1 gravimeter and 1 GNSS antenna, the campaign would take 2340 h. This means that in roughly one and half years time all caves with radius greater 25 m would be detected.

8. Discussion

The gravimetric method suffers from being non-unique, with infinite solutions explaining the observations. The solution can made to be unique, when constraints on geometry, depth and density of the causative body are possible. The example we show is a benchmark dataset which can be used to test methods that manage to find a solution to the inverse problem, reducing the non-uniqueness of the potential field method, because next to the field, the density of the causative body is exactly known, as well as depth and geometry.

In karstic areas the gravity method proves useful because the sheer existence of a cave is important for logistic reasons and in the frame of infrastructure and

urban development. With no constraints the volume can be estimated by applying the Gauss law, a classical method to define the total mass of the causative body. Knowing the density, the volume can be estimated, as long as the full signal of the anomaly is covered by the observations. When defining the body of an unknown karstic void, the density of the inside is always zero, the density of the calcareous rocks can be sampled at the surface, and the karstic evolution implies that the top of the cave is in a range between a few meters and a few tens of meters. The potential field method in this case becomes deterministic and proves useful in defining the position of the underground caves. Setting G the gravitational constant, ρ density of the Karstic limestones, $g(i,j)$ the grid of Bouguer anomalies with sampling dx, dy and size N by M and V the volume of the cave, the Eq. (9) can be solved for finding the volume of the cave.

$$\sum_{i=1,j=1}^{i=N,j=M} g(i,j)\mathrm{d}x\mathrm{d}y = -2\pi G\rho V \qquad (9)$$

From Eq. (9) and setting density equal to 2680 kg/m^3 (Pivetta and Braitenberg 2015), for our survey the volume comes out to be 180,690 m^3, corresponding to a missing mass equal to 4.8606×10^8 kg. Although this value is half the value derived from the laserscan (360,000 m^3), it shows that the gravimetric method is useful in defining the order of magnitude of the volume of the cave. The smaller estimated volume is due to the fact that the survey does not extend over the entire anomaly but is limited in extent.

An inversion with prisms is able to recover the geometry of the cave. Parameters are the density contrast between the calcareous rocks and the air and the assumed depth of the cave. A greater depth requires a greater volume to explain the observations.

Up to now we have considered void caves, but it cannot be excluded that a cave be filled with sediments. In this case the density contrast between the encasing rock and the cave is smaller, with a proportional reduction in the gravity signal. The size of the smallest cave we can detect will then depend on the percentage of sediment filling and the density contrast between sediments and the encasing rocks. Given a certain measurement noise level and a given station spacing, the smallest cave we can detect will be bigger compared to our above calculations. For the sediment filled caves a specific modeling should be accomplished in order to find the resolution power of the method.

The sediments could be present also above the cave, for instance due to a Quaternary covering or due to a sediment basin above the cave. The wavelengths describing the size of the Quaternary sheet or the basement morphology below the basin are much larger than the dimension of a cave. The gravity signal generated by the sedimentary cover is thus much broader than the signal of the cave. The two can then be separated by low–high pass filtering methods or by fitting a polynomial function to the long wavelength changes of the gravity map. Therefore a sedimentary sheet above the cave would not affect our conclusions because we can assume that the two signals can be efficiently separated.

9. Conclusions

Underground cavities bear a hazard when man-made constructions are built on the surface, due to their eventual development into sink holes. This work is dedicated towards defining the detectability of underground cavities with the gravimetric method by considering today's measuring capabilities. The detection level of terrestrial as well as of airborne measurements is considered. Here we document the gravimetric campaign of a benchmark dataset which contains the precise geometry of the cave and the terrain above it and the gravity measurements. The dataset can be used as a realistic example of the gravity of a natural cavity for potential field testing of forward and inverse methods. The challenges we have encountered in the measuring campaign due to the fact that the height measurements had to be done integrating GNSS methods and Total Station are typical of every gravity campaign that meets vegetation masking the GNSS signal. The fast RTK acquisition technique has been found to be sufficient for the purpose of the data acquisition, and is preferable due to the ease in acquiring the position of the gravity stations. The error level in height is near

to 1 cm, leading to a contribution of 0.003×10^{-5} m/s^2 in the gravity error. We have also shown that for campaigns with smaller precision requirements, the use of non-geodetic single frequency receivers, like the u-blox EVK-6T, is also possible, however in this case raw GNSS observations should be opportunely treated with non commercial softwares. Here the height is acquired with a standard deviation of 8 cm which affects the gravity measurements at the level of 0.02×10^{-5} m/s^2. The non geodetic receiver has the advantage of much lower cost with respect to the geodetic GNSS receivers. Ideally an area affected by karstification should be investigated systematically in order to map the existing cavities. The fastest way to cover the area is by airborne acquisition, and the simulations show that the helicopter acquisition is precise enough to detect, at least in principle, caves as large as our benchmark cave, that is with a dimension of 100 m length, and 60 m across and 100 m high. However, it should be reminded that during a real acquisition campaign possible mis-modeling of topographical effects as well as not ideal situation during the helicopter flight could easily mask the small signal due to the cave. Fixed wing aircraft cannot detect the cave as the noise level is too high. On the contrary, systematic terrestrial acquisition can detect much smaller caves, with radius down to 5 m. In order to be sure to detect all existing caves the station grid spacing depends on the minimum size of the cave to be detected. An acquisition that includes a density of three stations every square tile of 250 by 250 m^2 would catch caves with radius greater than 25 m, and top at 10 m depth. For the Classical Karst such campaign would take one and a half years with five gravimeters. If the caves are expected to be more superficial the smallest detectable size decreases by a small amount. The simulations show that a systematic investigation is ideally fulfilled with terrestrial measurements, using a gravimeter and GNSS methods for data acquisitions. A systematic investigation aiming to detect at least the largest caves of an area can be fulfilled with a low and slow flying helicopter. Once the suspicious anomalies are identified, the precise terrestrial campaigns can be fulfilled in the focus area, reducing the total amount of measurements to be taken.

Acknowledgments

We acknowledge the former director of the Grotta Gigante cave, Arch. A. Fabbricatore, for providing us the laserscan data and for the logistic support. The guides of the Grotta Gigante are gratefully thanked for their support in the density sampling campaign. The authors acknowledge Prof. Daisuke Yoshida of Osaka City University, and Dr. Eugenio Realini and Dr. Stefano Caldera of GReD for providing the u-blox data collected under the JSPS KAKENHI Grant Number 26730156. We thank Dr. S. Cirilli and Dr. F. Raicich for providing tide gauge data of Trieste harbor. We thank Thomas Jahr and an anonymous reviewer for the meticulous reviews.

References

A. Marussi GNSS network (2015), The GNSS stations are described in the home page of the network, http://www.regione.fvg.it/rafvg/cms/RAFVG/ambiente-territorio/strumenti-per-conoscere/FOGLIA1/.

Battaglia, M., Zuliani, D., Pascutti, D., Michelini, A., Marson, I., Murray, M.H., and Burgmann, R. (2003), *Network Assesses Earthquake Potential in Italy's Southern Alps*, Eos *84*, 262–264.

Braitenberg, C., Romeo, G., Taccetti, Q., Nagy, I. (2006), *The very-broad-band long-base tiltmeters of Grotta Gigante (Trieste, Italy): secular term tilting and the great Sumatra-Andaman Islands earthquake of December 26, 2004*, J. of Geodynamics *41*, 164–174.

Braitenberg, C., and Zadro, M. (2007), *Comparative analysis of the free oscillations generated by the Sumatra-Andaman Islands 2004 and the Chile 1960 earthquakes*, Bulletin of the Seismological Society of America *97*, S6–S17 doi: 10.1785/0120050624.

Braitenberg, C., and Nagy, I. (2014), *Illustrating the superposition of signals recorded by the Grotta Gigante pendulums with musical analogues*, Acta Carsologica *43/1*, 139–147.

Caldera, S., Realini E., Barzaghi R., Reguzzoni M., and Sansò F. (2015), *An experimental study on low-cost Geodetic monitoring*, Submitted to Journal of Surveying Engineering.

Cucchi, F., Casagrande, G., Manca, P., and Zini, L. (2001), *Il Timavo ipogeo tra l'Abisso di Trebiciano e la Grotta Meravigliosa di Lazzaro Jerko*, Le Grotte d'Italia 2, 39–48.

Davis, P. J., Interpolation and approximation (Courier Corporation, Mineola 1975).

Demeure, C. J., and Scharf, L. L. (1987), *Linear statistical models for stationary sequences and related algorithms for Cholesky factorization of Toeplitz matrices*, Acoustics, Speech and Signal Processing, IEEE Transactions *35*, 29–42.

Department Of Primary Industries, Victoria (2012), Gippsland Nearshore Airborne Gravity Survey—Data Package.

Devoti, R., Zuliani, D., Braitenberg, C., Fabris, P. and Grillo, B. (2015), *Hydrologically induced slope deformations detected by*

GPS and clinometric surveys in the Cansiglio Plateau, southern Alps, Earth and Planetary Science Letters *419*, 134–142, doi:10.1016/j.epsl.2015.03.023.

Farr, T.G., Rosen, P.A., Caro, E., Crippen, R., Duren, R., Hensley, S., Kobrick, M., Paller, M., Rodriguez, E., Roth, L., Seal, D., Shaffer, S., Shimada, J., Umland, J., Werner, M., Oskin, M., Burbank, D., and Alsdorf, D. (2007), *The Shuttle Radar Topography Mission*, Rev. Geophys. *45*, RG2004, doi:10.1029/2005RG000183.

Fingolo, M., Facco, L., Ceccato, A., Breganze, C., Paganini, P., and Cezza, M. (2011), *Tra realta' virtuale e rilievi 3D ad alta risoluzione*, Veneto Geologi *75*, 21–25.

Ford, D. and Williams, P., Karst Hydrology and Geomorphology, (Wiley, Chirchester, 2007).

Franklin, J. N. (1965), *Numerical simulation of stationary and non-stationary Gaussian random processes*, SIAM review *7*, 68–80.

Geonet (2015), http://sourceforge.net/projects/geonet/?source=directory, last access September 1, 2015.

Harlan, R. B. (1968), *Eotvos corrections for airborne gravimetry*, Journal of Geophysical Research *73*, 4675–4679.

Heiskanen, W. A., and Moritz, H. Physical Geodesy, (Technical University, Graz 1981).

Herrera, A. M., Suhandri, H. F., Realini, E., Reguzzoni, M., and de Lacy, M. C. (2015), goGPS: open-source MATLAB software. GPS Solutions, 1–9.

Hofmann-Wellenhof, B., Lichtenegger, H., and Wasle, E., GNSS–global navigation satellite systems: GPS, GLONASS, Galileo, and more, (Springer Wien New York, Wien 2008).

Lawson, C. L., and Hanson, R. J., Solving least squares problems (Prentice-Hall, Englewood Cliffs 1974).

Leick, A. GPS satellite surveying (Wiley, Hoboken 2004).

Li, B., Verhagen, S. and Teunissen, P.J.G., GNSS Integer Ambiguity Estimation and Evaluation: LAMBDA and Ps-LAMBDA, In China Satellite Navigation Conference (CSNC) 2013 Proceedings, Lecture Notes in Electrical Engineering 244 (eds. Jiadong, S., Wenhai, J., Haitao, W., and Chuang, S.) (Springer, Berlin 2013) pp. 291–301.

Paganini, P., and Pavan, A. (2012), *Rilievo laser-scanner della Grotta Gigante: Relazione Tecnica, Progressione*. Supplemento semestrale ad "Atti e memorie" *58*, 129–132.

Park, J., Song, T. A., Tromp, J., Okal, E., Stein, S., Roult, G., Clevede, E., Laske, G., Kanamori, H., Davis, P., Berger, J., Braitenberg, C., van Camp, M., Lei, X., Sun, H., Xu, H., and Rosat, S. (2005), *Earth's free oscillations excited by the 26 december 2004 Sumatra-Andaman earthquake*, Science *308*, 1139–1144.

Pivetta, T., and Braitenberg, C. (2015), *Laser-scan and gravity joint investigation for subsurface cavity exploration—the Grotta Gigante benchmark*, Geophysics *80*, B83–B94.

Rossi, L., Sampietro, D., and Sansò, F. (2012), GeoNet: un software per la compensazione di reti topografiche integrate, Proceedings of 16th National conference ASITA, 1157–1164.

Realini, E., and Reguzzoni, M. (2013), *goGPS: open source software for enhancing the accuracy of low-cost receivers by single-frequency relative kinematic positioning*, Measurement Science and Technology *24*, 115010.

Shako, R., Förste, C., Abrikosov, O., Bruinsma, S., Marty, J. C., Lemoine, J. M., and Dahle, C., EIGEN-6C: A high-resolution global gravity combination model including GOCE data, In Observation of the System Earth from Space-CHAMP, GRACE, GOCE and future missions (eds. Fletchner, F., Sneeuw, N., and Schuh, W-D.) (Springer, Berlin 2014) pp. 155–161.

Tenze, D., Braitenberg, C., and Nagy, I. (2012), *Karst deformations due to environmental factors: evidences from the horizontal pendulums of Grotta Gigante, Italy*, Bollettino di Geofisica Teorica ed Applicata *53*, 331–345, doi:10.4430/bgta0049.

Tsuji, H., Miyagawa, K., Yamaguchi, K., Yahagi, T., Oshima, K., Yamao, H., and Furuya, T. (2013), *Modernization of GEONET from GPS to GNSS*, Bulletin of the Geospatial Information Authority of Japan *61*, 9–20.

Uieda, L., Ussami, N., and Braitenberg, C. F. (2010), *Computation of the gravity gradient tensor due to topographic masses using tesseroids*, EOS, Trans. Am. Geophys. Un., *91*(26).

Uieda, L., Bomfim, E. P., Braitenberg, C., and Molina, E. (2011), Optimal forward calculation method of the Marussi tensor due to a geologic structure at GOCE height, Proc. of '4th International GOCE User Workshop', Munich, Germany, 31 March–1 April 2011 (ESA SP-696, July 2011).

Verhagen S., and Li B. (2012), LAMBDA—Matlab implementation, version 3.0, Delft University of Technology and Curtin University.

Visintin, L. (2011), Realizzazione di un SIT finalizzato allo studio delle aree carsiche, PhD Thesis, University of Trieste, Trieste, http://www.openstarts.units.it/dspace/handle/10077/4513.

Wanninger, L. (2003), *Virtual reference stations (VRS)*, GPS Solutions *7*, 143–144.

Watson, G. N., A treatise on the theory of Bessel functions (Cambridge University Press, Cambridge 1995).

Zadro, M., and Chiaruttini, C. (1975), Loading effects of the Mediterranean tides, Proc. of the Seventh International Symposium on Earth Tides, Sopron, 1973. (Akademiai Kiado, Budapest) pp 405–501.

Zanolla, C., Coren, F., Cucchi, F., Giorgetti, F., and Lovo, M. (1996), *Elaborazione dei dati gravimetrici in corrispondenza della Grotta Gigante (Carso Classico, Trieste, Italia)*, Atti e Memorie della Commissione Grotte "E. Boegan" *33*, 17–24.

Zuliani, D., Battaglia, M., Pascutti, D., Murray, M., Burgmann, R., Michelini, A., and Marson, I. (2003), FReDNet: a continuous GPS geodetic network to monitoring crustal deformation in NE Italy, EGS-AGU-EUG Joint Assembly 1, 2120.

(Received July 27, 2015, revised September 19, 2015, accepted September 24, 2015, Published online October 11, 2015)